JAST
Journal of Aerospace Science and Technology

Pages: 1-15/ Vol. 16/ No. 1 /Winter- Spring 2023

Journal of Aerospace Science and Technology

www:jast.ias.ir

Scientific-Research Article

Design and Analysis of a Fuzzy PID Controller In Comparison with Other Controllers for Pitch-Yaw Gimbal

Amir Moghtadaei Rad [1]
1-Department of Electrical Engineering Islamic Azad University of Hashtgerd

ABSTRACT

***Keywords**: Fuzzy Controller, PID, Stabilized platform, Frequency Domain*

In this paper, a complete model, including the cross-coupling of the azimuth and elevation axes, the effect of axis friction, non-perpendicularity, and imbalance of the axes, was implemented for a platform with two degrees of freedom. Since this model includes three loops of current, stability, and tracking from the inside to the outside, it is necessary to design a suitable controller for each loop separately from the inside to the outside after linearizing the obtained model. Also, due to two channels, azimuth and elevation, it was necessary to repeat and design three controllers for both channels separately. Since this article aims to compare the performance of different controllers, PID, Fuzzy, Fuzzy PID, and Fuzzy self-tuning controllers for both channels and all loops, their design and implementation in time domains were analyzed. In the end, the relative advantages of each controller according to different parameters of the system were presented in a comparative table and shown that each has advantages and disadvantages depending on angular rates and disturbances.

Introduction

Imaging sensors, such as radars, cameras, infrared (I.R.) sensors, lasers, and so forth, are widely used in different fields of industry for safety, target tracking, astronomical telescopes, obstacle detection, and more. Inertial Stabilized Platforms (ISP) have been introduced to isolate these devices from vehicle motion and external disturbances.
In this study, (ISPs) have been introduced. An ISP is a mechanism involving gimbal assemblies controlling the inertial orientation of the payload, and a target tracker that involves image processing techniques. Therefore, the fundamental objective of an ISP, when used with optical equipment, is to obtain good-quality shots of the target and its surrounding area. The control strategies of these platforms consist of two parts—high-level (outer loop) and low-level (inner loop) [1]. The stabilization system continuously maintains the tracking sensor's line of sight (LOS) toward the target by isolating the sensor from operating environmental disturbances. Stabilization of the tracking sensors (such as antennas or telescopes) is usually achieved by placing the antenna in a two-axis gimbal and placing a two-axis rate sensor in the inner gimbal [2]. A DC motor actuates the gimbal axis. The angular speed or rotation rate of the gimbal axis sensed by the rate gyro is compared with an input rate command. The

1 Assistant Professor (Corresponding Author) **Email: *** amir.moghtadaei@yahoo.com

DOI :10.22034/jast.2023.377460.1140
Submit: 19/12/2022 / Accepted: 11/03/2023
Print ISSN:1735-2134 Online ISSN: 2345-3648

difference between the gimbal rate (LOS rate) and the input rate (the rate error) is supplied to a controller from which a control signal is generated to drive the dc motor, which produces the required torque to turn the gimbal to follow the rate command. Thus, the stabilization loop in target tracking forms a control system in which the controller aims to make the rate error zero when the gimbal follows the rate command.

As the gimbal system is attached to a base or vehicle body, the control system has to isolate the tracking sensor (antenna) from base motion. The overall control system for the two-axis gimbal can be constructed with two stabilization loops, as shown in Figure 1, where inner (elevation) and outer (azimuth) gimbals correspond to pitch and yaw axes, respectively.

In the stabilization loop, a DC motor must produce an amount of torque proportional to the control signal input from the controller. The control of LOS inertial stabilization systems is a complex problem because of the precise requirement of providing accurate target tracking and pointing in the dynamic operating environment and the presence of cross-coupling between the two gimbal axes in the system [3].

In [4], the kinematics and geometrical coupling relations for the two degrees of freedom gimbal assembly have been obtained for a simplified case when each gimbal is balanced and the gimballed element's bodies are suspended about their principal axes. Equations of motion for the two axes' gimbal configuration have been discussed, assuming that the gimbals are rigid bodies with no mass imbalance [2].

A novel method to measure unbalanced moments in a two-axes gimbaled seeker has been presented by Yu and Zhao in [5]. But this method needed to be improved for the better performance of a seeker owing to the limited sensor's accuracy.

In both [2] and [6], the dynamical models of the elevation and azimuth gimbals were derived on the assumption that the gimbals' mass distribution was symmetrical concerning their frame axes. Therefore, the products of inertia were neglected, and the model was simplified. Many papers have studied two axes of gimbal systems, and the gimbal system model has been obtained utilizing different approaches.

However, most of these studies have considered that the elevation and azimuth channels are identical. That is why, only one axis was simulated and tested. Thus, the cross-coupling, caused by the base angular motion and the properties of gimbal system dynamics – has been ignored.

Controlling LOS stabilizer systems is complicated because of cross-coupling between channels [7].

The problem with gimbal system control is the cross-coupling between two control loops. Cross-coupling can describe the characteristics of a dynamic gimbal system and its reflection when the azimuth gimbal affects elevation gimbal even when its body is nonrotating [8].

A robust control is suggested to stabilize and control the two-axis gimbal system [9]. A robust PI controller is applied to enhance high performance and appreciable stabilization [8]. An adaptive fractional-order sliding mode controller stabilizes a two-DOF gimbal system [10]. The inverse system method with the inertial model control is utilized because of the system's nonlinearity and coupling terms [11]. To enhance the tracking and stabilization of the ISP, an adaptive decoupling control based on a neural network is suggested [12]. To ensure the stability of the design, a fuzzy controller is proposed for the two-axis gimbal system [13]. ~~A~~daptive feedback linearization is utilized to stabilize these systems [14].

Many works have been done in this area, such as Do Li, David Hullender, and Mike Direnzo [15] proposed a nonlinear induced disturbance rejection, H. Ambrose, Z. Qu, and R. Johnson [16] proposed a robust nonlinear control, T.H. Lee, E.K. Koh, M.K. Loh. [17] proposed a stable adaptive control, and Bo Li and David Hullender [18] proposed a self-turning controller for a nonlinear inertial stabilization system. Jasim Ahmed and Dennis S. Bernstein worked on adaptive control for a system with an unbalanced rotor.

Also, LQG control [19], adaptive control [20], H∞ control [21], and hybrid control [22].

This paper is divided into seven parts. The first introduces the structure and principle of a two-axis gimbaled ISP for stabilizing LOS. In the next section, the cinematic relation between them will be considered. Then the dynamical equation of the 2-DOF system for elevation and azimuth stabilizing gimbal.

According to Abdo and Tolooei [23] will be represented. The third section presents a real and practical model by noticing nonlinearities, especially friction, coupling, and unbalancing.

Section four begins with the representation of a linear and practical model of a DC motor and gyro. Then, the model will be validated by doing the experimental test to identify the system and by comparing the result and the presented model with a numerical value. Section five assigns to studying the performance of the stabilization loop by using the designed PID, Fuzzy PID, Self Tuning Fuzzy PID controller.
This compensator for the tracking loop will be designed for the desired implication of this built ISP in section 6. Finally, the frequency response of two elevation and azimuth channels will be analyzed, and the bandwidth of each loop will be determined.
In the seventh section, the conclusion of this paper will be represented

Cinematic and Dynamic Relations of 2-Dof Pitch-Yaw Gimbal

A typical configuration of a 2-DOF gimbal system is shown in Figure 1. A gyro sensor is fixated to the inner platform of the gimbal system (pitch channel); its measurements help stabilize the LOS through feedback control schemes [1]

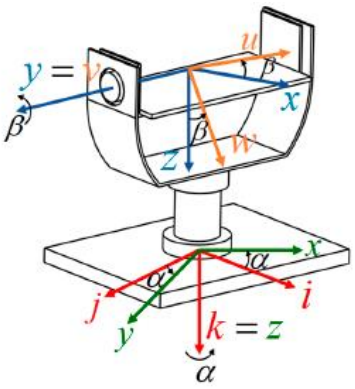

Figure 1. The Two-Axis Gimbal System.

Three reference frames are introduced to facilitate the dynamic modeling of the gimbal system [2] First. Frame B is a frame fixed to the body with its axes $(\vec{\imath},\vec{\jmath},\vec{k})$.The frame γ is fixed to the azimuth gimbal and defined by the axes $(\vec{x},\vec{y},\vec{z})$.Finally, the frame P is fixed to the elevation gimbal with the coordinates $(\vec{u},\vec{v},\vec{w})$. The center of rotation of the frames is located at the origin. Frame B is fixed to the body of the gimbal and is carried to coincidence with the yaw gimbal frame γ by the positive angle α (around the k-axis). On the other hand, the yaw gimbal frame γ is carried into coincidence with the pitch gimbal frame P by the positive angle β (around the y-axis).

The transformation matrices F_{YB} and F_{PY} are the transformation between the base and the yaw frame and between the yaw and the pitch channels. These matrices are defined based on the previously stated rotations [1].

$$F_{\gamma\beta} = \begin{bmatrix} \cos\alpha & \sin\alpha & 0 \\ -\sin\alpha & \cos\alpha & 0 \\ 0 & 0 & 1 \end{bmatrix} \quad (1)$$

$$F_{P\gamma} = \begin{bmatrix} \cos\beta & 0 & -\sin\beta \\ 0 & 1 & 0 \\ \sin\beta & 0 & \cos\beta \end{bmatrix}$$

Corresponding inertial angular rates of the frames B, γ, and P are given, respectively, as

$$\vec{\omega}_B = \begin{bmatrix} \omega_i \\ \omega_j \\ \omega_k \end{bmatrix} \quad \vec{\omega}_\gamma = \begin{bmatrix} \omega_x \\ \omega_y \\ \omega_z \end{bmatrix} \quad \vec{\omega}_p = \begin{bmatrix} \omega_u \\ \omega_v \\ \omega_w \end{bmatrix} \quad (2)$$

where ω_i , ω_j , ω_k are the base angular velocities of the B frame, ω_x , ω_y , ω_z are the angular rates of the γ frame, and ω_u , ω_v , ω_w are the angular rates of the P frame. The angular velocities of the two gimbals expressed in the adjacent frame are calculated as

$$\begin{bmatrix} \omega_x \\ \omega_y \\ \omega_z \end{bmatrix} = F_{\gamma\beta} \begin{bmatrix} \omega_i \\ \omega_j \\ \omega_k \end{bmatrix} + \begin{bmatrix} 0 \\ 0 \\ \dot{\alpha} \end{bmatrix} = \begin{bmatrix} \omega_i \cos\alpha + \omega_j \sin\alpha \\ -\omega_i \sin\alpha + \omega_j \cos\alpha \\ \omega_k + \dot{\alpha} \end{bmatrix} \quad (3)$$

$$\begin{bmatrix} \omega_u \\ \omega_v \\ \omega_w \end{bmatrix} = F_{p\gamma} \begin{bmatrix} \omega_x \\ \omega_y \\ \omega_z \end{bmatrix} + \begin{bmatrix} 0 \\ \dot{\beta} \\ 0 \end{bmatrix} = \begin{bmatrix} \omega_i \cos\alpha + \omega_j \sin\alpha \\ -\omega_i \sin\alpha + \omega_j \cos\alpha \\ \omega_k + \dot{\alpha} \end{bmatrix} \quad (4)$$

Inertia matrices of elevation and azimuth gimbals are;

$$J_\gamma = \begin{bmatrix} \gamma_x & \gamma_{xy} & \gamma_{xz} \\ \gamma_{xy} & \gamma_y & \gamma_{yz} \\ \gamma_{xz} & \gamma_{yz} & \gamma_z \end{bmatrix} \quad J_P = \begin{bmatrix} p_u & p_{uv} & p_{uw} \\ p_{uv} & p_v & p_{vw} \\ p_{uw} & p_{vw} & p_w \end{bmatrix} \quad (5)$$

Where $J_{P.}$ and $J_{Y.}$ are, respectively, the inertia matrix of the pitch and the yaw channel.

Modeling of 2-DoF Pitch-Yaw Gimbal

According to Newton's second law, if a torque T is applied to a homogenous rigid mass with a moment of inertia J, then the body develops an angular acceleration according to the following relation; T = J.a. Therefore, if the applied torque is zero the controlled object can be prevented from rotating. If we consider the azimuth and the elevation gimbals as rigid bodies, then the motion equations of the gimbal system can be elaborated. Thus, the external torques applied to the gimbal channels are derived from the following relation;

$$T = \frac{d}{dt}\vec{H} + \vec{\omega} \times \vec{H} \quad \vec{H} = J.\vec{\omega} \quad (6)$$

Where $\vec{H}$ is the angular momentum. Based on equation (6), the pitch gimbal dynamic model is derived as follows;

$$P_v\dot{\omega}_v = T_E + T_{DE1} + T_{DE2} \quad (7)$$

where T.E. is the total external torque applied about the v-axis of the pitch gimbal, and TDE1 represents the inertia disturbances generated by the base rotation. TDE2 represents the cross-coupling resulting from the relative motion between the base and the azimuth channel. The derived expressions of these disturbances are such;

$$\begin{aligned} T_{DE1} &= -[P_{uv}\,cos\beta + P_{vw}\,sin\beta]\left(\omega_x + \omega_y + \omega_z\right) \\ &+ [P_{vw}\,cos\beta - P_{uv}\,sin\beta]\omega_y\omega_x + [(P_u - P_w)cos2\beta \\ &- 2P_{uw}sin2\beta]\omega_x\omega_z + \frac{1}{2}[[(P_u - P_w)sin2\beta \\ &+ 2P_{uw}cos2\beta]\omega_x^2 \end{aligned} \quad (8)$$

$$\begin{aligned} T_{DE2} &= [P_{uv}\,sin\beta - P_{vw}\,sin\beta] - \frac{1}{2}[(P_u - P_w)sin2\beta \\ &+ P_{uw}cos2\beta]\omega_z^2 \end{aligned} \quad (9)$$

In the same manner, the dynamic model of the yaw channel is derived

$$\boldsymbol{J_{AZ}\,\omega_z = T_A + T_{DA1} + T_{DA2} + T_{DA3} + T_{DA4}} \quad (10)$$

T.E. is the total torque applied about the z-axis of the yaw gimbal, while JAZ is the moment of inertia. TDA1, TDA2, and TDA3 represent the inertia disturbances generated by the base rotation. TDA4 represents the cross-coupling from the relative motion influencing the azimuth and the elevation channels. The dynamic model expressions of these disturbances are listed as such;

$$J_{AZ} = Y_z + P_u\sin^2\beta + P_w\cos^2\beta - P_{uw}\sin(2\beta) \quad (11)$$

$$T_{DA1} = \omega_x\omega_y[\gamma_{xy} + P_u cos^2\beta + P_w sin^2\beta + P_{uw}\sin(2\beta) - (\gamma_y + P_v)] \quad (12)$$

$$\begin{aligned} T_{DA2} = &-\left(\omega_x - \omega_y\omega_z\right)[\gamma_{xz} + (P_w - P_u)cos\beta sin\beta \\ &+ P_{uw}\cos(2\beta)] \\ &- \left(\dot{\omega}_y + \omega_x\omega_z\right)\left[\gamma_{yz} - P_{uv}sin\beta\right. \\ &\left.+ P_{vw}\cos\beta\right] - (\omega_x^2 - \omega_y^2)[\gamma_{xy} \\ &+ P_{uv}cos\beta + P_{vw}sin\beta] \end{aligned}$$

$$\begin{aligned} T_{DA3} = &\dot{\omega}_y[P_{vw}\cos\beta - P_{uv}sin\beta] + [(P_u - \\ &P_w)\cos(2\beta) + 2P_{uw}\sin(2\beta) - P_v]\dot{\beta}\,\omega_x + [(P_u - \\ &P_w)\sin(2\beta) - 2P_{uw}\cos(2\beta)]\omega_y\omega_z - [P_{uv}cos\beta + \\ &[P_{vw}\sin\beta]\omega_y^2 \end{aligned} \quad (14)$$

$$\begin{aligned} T_{DA4} = &[P_{uv}sin\beta - P_{vw}\cos\beta]\dot{\omega}_v + [P_{uv}cos\beta + \\ &P_{vw}sin\beta]\omega_v^2 + [(P_w - P_u)\sin(2\beta) + \\ &2P_{uw}\cos(2\beta)]\omega_v\omega_z \end{aligned} \quad (15)$$

Using the expression of $\omega_w$in equation (4) to obtain ω_z and its derivative $\dot{\omega}_z$ and replacing these terms in equation (10) transforms it into a differential equation in terms of the angular velocity of the pitch frame ω_w [24]. Therefore, the resulting equation develops into

$$\begin{aligned} J_{AZ}\dot{\omega}_w = &(T_A + T_{DA1} + T_{DA2} + T_{DA3} + T_{DA4})cos\beta + \\ &J_{AZ}[\omega_x sin\beta + \omega_v(\omega_v - \omega_y)] \end{aligned} \quad (16)$$

Stabilization Loop Construction

The components of the stabilization loop are;

Table 1. D.C. Motor Specifications

Parameter	value
Nominal voltage	27v
No Load speed $\boldsymbol{\omega_{nl}}$	418 rpm
Terminal Resistance $\boldsymbol{R_a}$	2.6
Terminal inductance $\boldsymbol{L_a}$	$5.8 \times 10^{-3} H$
Torque constant $\boldsymbol{K_{TM}}$	$2.308\frac{Nm}{A}$
Back EMF $\boldsymbol{K_e}$	$0.23\ \frac{V}{rad/min}$
Rotor inertia $\boldsymbol{J_m}$	$0.0254\ kg.m^2$
Damping Ratio $\boldsymbol{a_m}$	0

As indicated in Fig. 2, the researchers tried to utilize and apply many modern techniques to control inertia stabilization systems; the conventional PID and its constructions are still the most used due to their simple structure, cheap costs, simple design, and high performance [26]. Therefore, two PI controllers (*KEL* for the elevation channel and *KAZ* for the azimuth one) have been utilized for comparison.

$$K(EL) = 0.59 + \frac{0.015}{z-1} \quad K(AZ) = 0.7 + \frac{0.002}{z-1} \quad (17)$$

Any servo motion control system should have an actuator module that makes the system perform its function. The most common actuator used to perform this task is the D.C. servomotor. D.C.

motor is one of the simplest motor types. It is widely preferred for high-performance systems requiring minimum torque ripple, rapid dynamic torque, speed responses, high efficiency, and good inertia [25]. These motors speedily respond to a command signal through a suitable controller. Speed control is carried out in this motor by changing its supply voltage [26]. D.C. motor from ERIC Company (160LYX05) (Table 4-1) is utilized. The transfer function of the D.C. motor can be obtained as follows;

$$G_m(s) = \frac{K_{TM}}{(L_a s+R_a).(J_m^* s+a_m^*)+K_e K_{TM}} \quad (18)$$

$$J_m^* = J_m + J_L$$
$$a_m^* = a_m + a_L = 0$$

where J_L is the platform's moment of inertia, and a_L is the load's damping ratio. The platform represents the motor load, which is attached to the output of the gears or directly to the shaft motor. The platform is modeled based on its moment of inertia J_L that depends on its dimensions and its position concerning the axis of rotation. In this paper, a discus is proposed to represent the platform where its mass *M(AZ)*= 210 kg and radius r = 44 cm, so $J_{LAZ} = 40.656\ kg \times m^2$ for the Azimuth channel. By subtracting the base mass from the mass of the whole body, the mass for the elevation channel is related to the camera only, so M(E.L.)= 65kg and J_{LEL} =16.25 $kg \times m^2$.

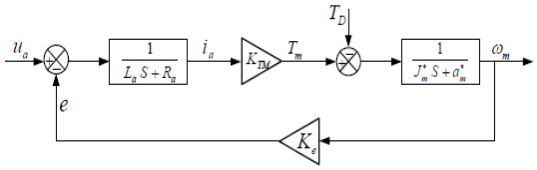

Figure 2. The General DC Motor block diagram [27].

This paper considers the 475 T rate gyroscope from the U.S. Dynamics company (Table 4-2). The rate gyro can typically be modeled (avoid extra spaces) in the second-order system [2-33]. For the gyro, natural frequency ω*n* = 50 Hz, and the damping ratio ζ= 0.7 and so the gyro transfer function is [23]

$$G_{gyro}(s) = \frac{2500}{s^2+70s+2500} \quad (19)$$

Table 2. Gyroscope Characteristic**.**

Performance:	
Input Rate	From ±40 to ±1000 °/sec
Input Excitation	7 to 26 VAC 16 to 36 VDC
Output	AC or DC
Scale Factor	To Customer Specification
Natural Frequency	20 Hz to 140 Hz
Damping Ratio	0.4 to 1.0
Linearity	< 1% Full Scale
Hysteresis	< 0.1 °/sec
Threshold	± 0.01 °/sec
Resolution	± 0.01 °/sec
Zero Rate Output (Bias)	< 0.1 °/sec
Bandwidth (-3 db)	Up to 100 Hz
G-Sensitivity	< 0.05 °/sec/g
Environmentals:	
Operating Temperature	-54° C to +95° C
Shock	300g
Vibration (20 to 2000 Hz)	20g rms

Also, Inertia matrices of elevation and azimuth gimbals are;

$$J_P = J_\gamma = \begin{bmatrix} \gamma_x & \gamma_{xy} & \gamma_{xz} \\ \gamma_{xy} & \gamma_y & \gamma_{yz} \\ \gamma_{xz} & \gamma_{yz} & \gamma_z \end{bmatrix}$$

$$= \begin{bmatrix} 4.065 & -0.4018 & -0.4650 \\ -0.4018 & 11.6366 & -0.08554 \\ -0.4650 & -0.08554 & 12.7792 \end{bmatrix} \quad (20)$$

Which are used in modeling and simulations.

The current controllers which are used in the current loop are as follows

$$K_{motor}(EL) = 12 \times \frac{z-0.9459}{z-1} \quad (21)$$
$$K_{motor}(AZ) = 10 \times \frac{z-0.8503}{z-1}$$

The configuration of the stabilization loop is as follows;

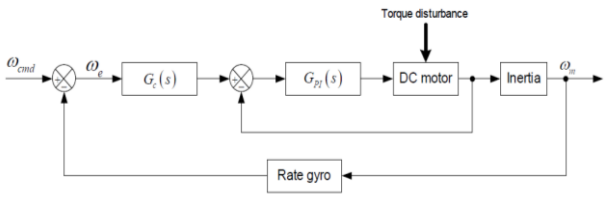

Figure 3. Stabilization loop model [25].

Controller System Design

The overall objective of a gimbal control strategy is to follow the desired trajectory in real-time in a short period, with a minimum steady-state error. Rapid and accurate performances require the design of robust control techniques.
So this paper compares three controllers, PID, Fuzzy PID, and Self-tuning Fuzzy PID, for the 2DOF platform and their performance in different conditions.

PID Controller Design

The drawback of the conventional PID appears when the control system works under variable conditions. Therefore, the PID controller can only perform well in systems such as the proposed inertia stabilization system if the controller parameters are returned. The progress report [28] Pointed out that the adaptive control technique is the future development direction of LOS inertia stabilization systems. In such environments, the overshoot in the gimbal system response is an inevitable challenge that must be solved because it degrades The control system performance. The solution Difficulty results from the overshoot and rise time usually conflict each other and cannot be reduced simultaneously.
The conventional PID controller and its different structures have been widely used for the speed control of D.C. motor drives and gimbal systems (especially PI controllers). Although the PI controller keeps a zero steady-state error to a step change in reference, it also has undesirable speed overshoot (high starting overshoot), slow response due to sudden changes in load torque, and sensitivity to controller gains [30].

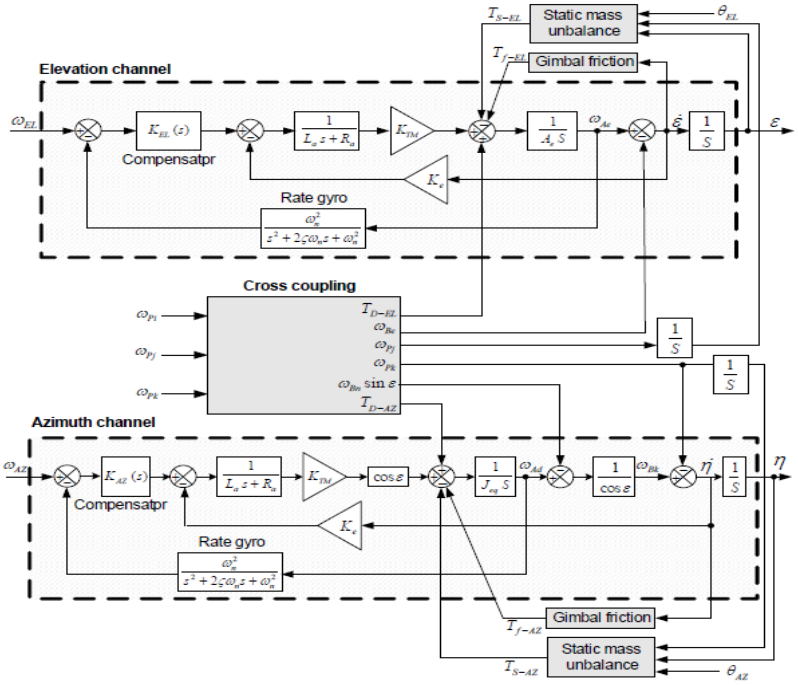

Figure 4. Yaw-Pitch Gimbal with Stabilization Loop [29].

Thus, utilizing conventional control approaches like classical PID (PI) can solve this problem approximately and slightly decrease the overshoot but absolutely at the expense of increasing the rise time value.

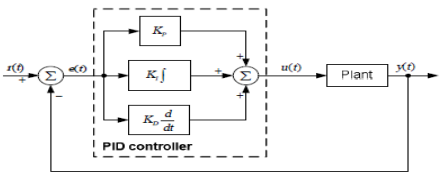

Figure 5. PID control Schematics.

The control law in PID is as follows;

$$u(t) = K_p + K_I \int e(\tau)d\tau + K_d \frac{de(t)}{dt} \qquad (22)$$

The controller and their response which MATLAB PID APP designs, are as follows;

$$K_{motor}(EL) = 12 \times \frac{z-0.9459}{z-1} \qquad (22)$$

$$K_{motor}(AZ) = 10 \times \frac{z-0.8503}{z-1} \qquad (23)$$

$$K_{Stab}(EL) = K_{Stab}(AZ) = 0.8 + \frac{0.002}{z-1} \qquad (24)$$

$$K_{Track}(EL) = K_{Track}(AZ) = 50 + \frac{0.025}{z-1} \qquad (25)$$

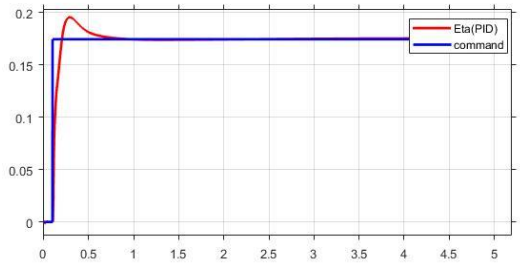

Figure 6. Azimuth angle step response.

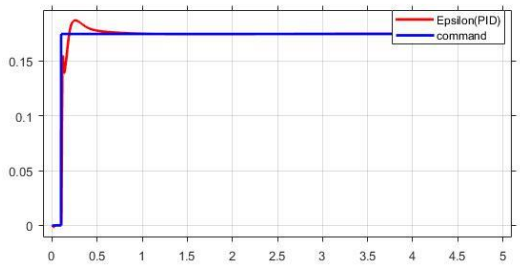

Figure 7. Elevation angle step response.

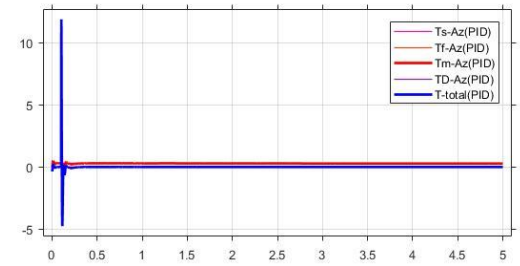

Figure 8. Azimuth Channel Torque response.

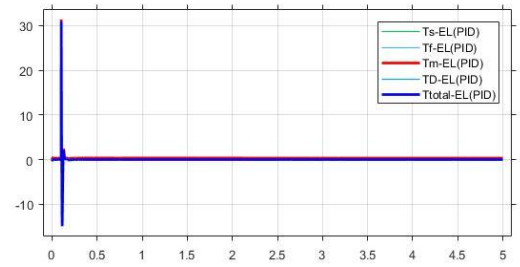

Figure 9. Elevation Channel Torque response**.**

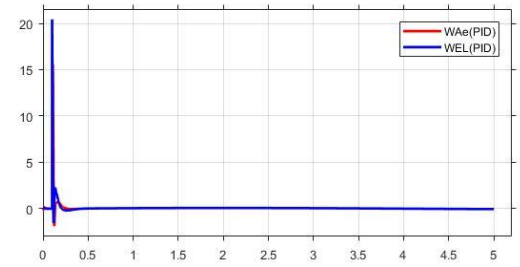

Figure 10. Azimuth rate angle response**.**

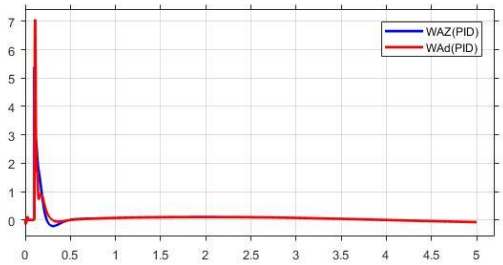

Figure 11. Elevation rate angle response

Fuzzy PID Controller Design

A fuzzy logic controller belongs to the intelligent control system, which combines the technique from the field of artificial intelligence with those of control engineering to design an autonomous system that can sense, reason and plan, learn and act intelligently [31]. The fuzzy controller comprises four main components, fuzzification interface, knowledge base, inference mechanism, and defuzzification interface [31]. Fig 12 shows components of the fuzzy logic controller. Fuzzification converts input data into suitable linguistic values, while defuzzification yields a non-fuzzy control action from inferred fuzzy control action. The rule base is a decision-making logic that simulates a human decision process, inters fuzzy control action from the knowledge of the control rules and linguistic variable definitions. The inference mechanism uses the fuzzified input variables to evaluate control rules stored in the fuzzy rule base. The result of this evaluation is a single fuzzy set or several fuzzy sets. Various structures of fuzzy PID (including PI and PD) controllers and fuzzy non-PID controllers have been proposed in the literature. The conventional fuzzy PID controller needs three inputs, and the rule base has three dimensions; it is more difficult to design the rule base.

On the other hand, the fuzzy PD type controller difficultly eliminates the steady state error, which can completely be removed using the fuzzy PI type controller. The fuzzy PI-type controller, however, performs poorly regarding the transient response, mainly when used for the higher-order process [32]. To obtain the advantages of the two controllers, they are combined to make a fuzzy PID type controller with just two inputs and a two-dimension rule base. Fig 13 shows the construction of the proposed fuzzy PID type controller, which will be utilized in this paper instead of the conventional PID. Where Ke, Kd is the input scaling factors of error and change of error and β,

α is the output scaling factors. Based on what has been made in [33]. The relation between input and output variables of fuzzy parameters is

$$U = A + PE + D\dot{E}; \quad E = K_e e\,, \dot{E} = K_d \dot{e} \qquad (26)$$

The output of the fuzzy PID type controller is

$$u_c = \alpha U + \beta \int U dt = (\alpha K_e P + \beta K_d D\,)e + (\beta K_e P) \int e(t)dt + (\alpha K_d D)\frac{de(t)}{dt} \qquad (27)$$

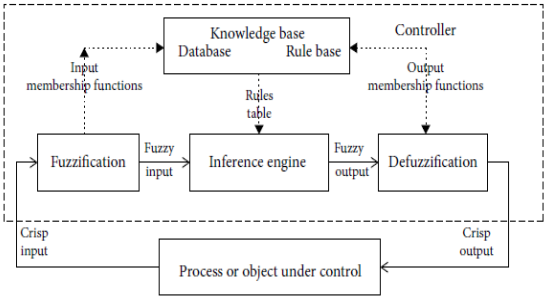

Figure 12. Components of Fuzzy Logic Controller**.**

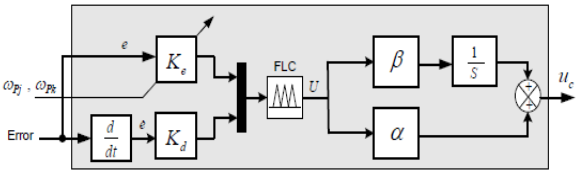

Figure 13. the model of the proposed Fuzzy PID controller (type-1).

In the fuzzification process, the triangular membership function is chosen for error, *e(t)* rate of change of error, de(t)/d*t*, and *U* variables with seven linguistic variables defined, namely, negative large (N.L.), negative medium (N.M.), negative small (N.S.), zero (Z.R.), positive small (P.S.), positive medium (PM), and positive large (P.L.) are shown in Figure 15.

The formation of fuzzy rules varies depending on the process and controller type. The rule base is chosen based on controller properties, nonlinear disturbances, DC motor characteristics, and gimbal payload. An approach for forming the rule base is as follows; when the difference between the desired output and the system output is too large, the error value needs to be reduced so that the system output reaches the desired value rapidly; thus, the desired rule base is if *e*(t) is P.L. and d*e(t)*/d*t* is Z.R., then the control variable *U* is selected to be P.L. If the error *e(t)* is Z.R. and d*e*(t)/d*t* is nonzero, then *U* should not be zero (for example, if *e* is Z.R. and d*e*/d*t* is N.L., then *U* is N.L.). When the system output reaches the desired value, both *e(t)* and d*e*(t)/d*t* are zero; thus, there is no need for control input; therefore, *U* should be selected as Z.R. The complete rule base contains 49 rules based on the above approach and is shown in Table 5. For analyzing the performance of fuzzy PID controller with 49-rule Mamdani method. another rule base is considered with 25 rules, similar to the one with 49 rules, except for the linguistic variables N.M. and PM (type-2).

Table 3. Fuzzy PID rules for input and output variables

de(t)/dt								
e(t)		NL	NM	NS	ZR	PS	PM	PL
	NL	NL	NL	NL	NL	NM	NS	ZR
	NM	NL	NL	NL	NM	NS	ZR	PS
	NS	NL	NL	NM	NS	ZR	PS	PM
	ZR	NL	NM	NS	ZR	PS	PM	PL
	PS	NM	NS	ZR	PS	PM	PL	PL
	PM	NS	ZR	PS	PM	PL	PL	PL
	PL	ZR	PS	PM	PL	PL	PL	PL

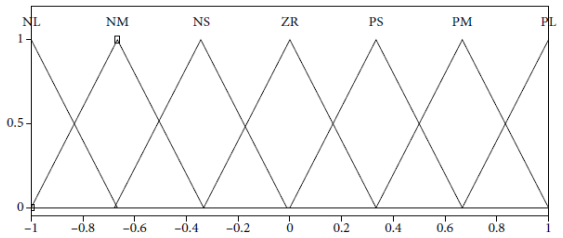

Figure 14. Membership Functions for input and output variables

The behavior of a two-axis gimbal system with fuzzy PID controllers is analyzed in MATLAB/Simulink.

To establish the online tuning of K_e, a parametric study is applied to obtain the most suitable value of K_e against every value of the angular velocities ω_{pj}, ω_{pk} along the interval [0-15] deg/sec. Based on this parametric study, two relations are obtained for elevation and azimuth channels as follows

$$K_e(\omega_{pk}) = -0.0013\omega_{pk}^2 - 0.0057\omega_{pk} + 0.6293 \qquad (28)$$

$$K_d(\omega_{pk}) = 0.005 \quad \beta = 25 \quad \alpha = 50$$
$$K_e(\omega_{pj}) = -0.0013\omega_{pj}^2 - 0.0057\omega_{pj} + 0.6293 \qquad (29)$$
$$K_d(\omega_{pj}) = 0.0005 \quad \beta = 25 \quad \alpha = 50$$

The results are as follows;

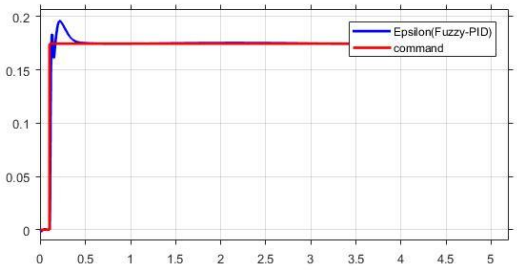

Figure 15. Elevation angle step response.

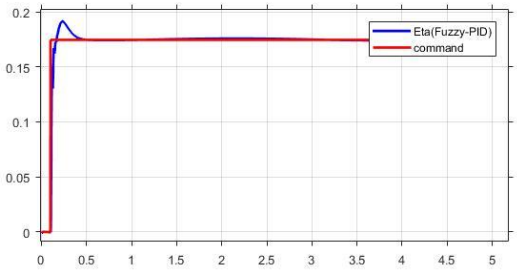

Figure 16. Azimuth angle step response.

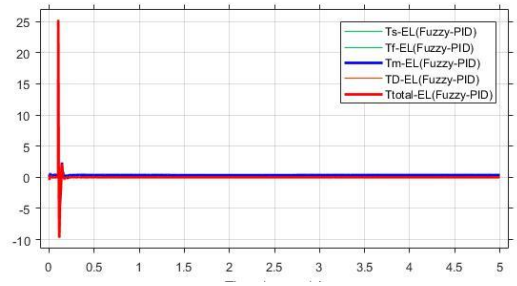

Figure 17. Elevation Channel Torque response

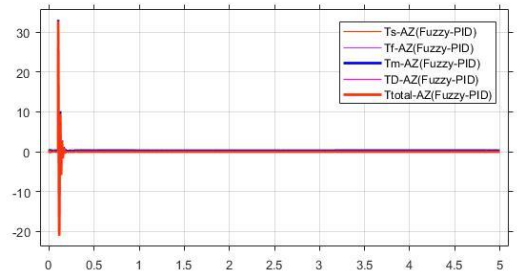

Figure 18. Azimuth Channel Torque response**.**

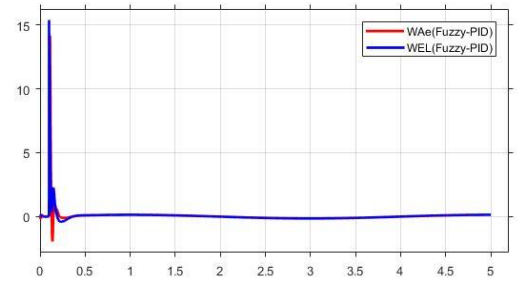

Figure 19. Elevation rate angle response**.**

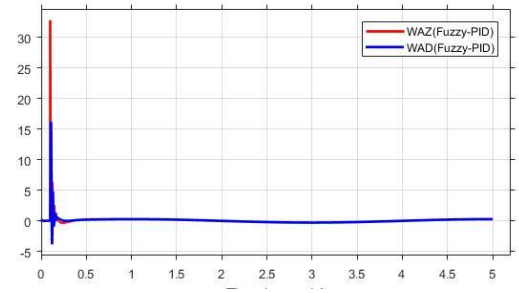

Figure 20. Azimuth rate angle response.

Self-Tuning Fuzzy PID Controller Design

As described previously, the adaptation of $K_p(t)$, $K_i(t)$, and $K_d(t)$ follows the adaptation of $\Delta e_p(t)$, $\Delta e_i(t)$, and $\Delta e_d(t)$. Hence, the key to designing an implicit adaptive PID controller is to develop the adaptation law to obtain the signals $\Delta e_p(t)$, $\Delta e_i(t)$, and $\Delta e_d(t)$.

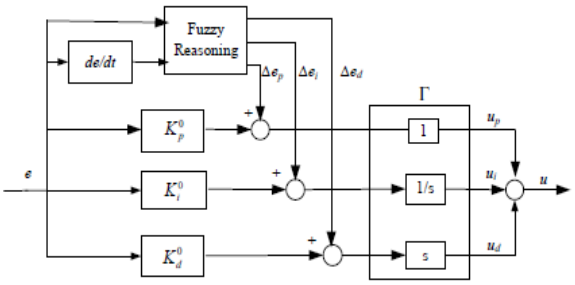

Figure 21. the model of the proposed self-tuning Fuzzy PID controller (type-2).

To produce the signals $\Delta e_p(t)$, $\Delta e_i(t)$, and $\Delta e_d(t)$, FLC is used in this paper. The design of the FLC is discussed in the following.

Like the commonly-used FLC, the FLC has two inputs. One is the system error $e(t)$, and the other is its change $\dot{e}(t)$To produce the three signals, the FLC needs three outputs. Consequently, the FLC in this paper has two inputs and three outputs, as shown in Fig 21.

In a fuzzy logic system, the membership function is the operation that translates crisp input data into a membership degree. In this paper, all the fuzzy sets of the inputs and outputs of the FLC are *{*NB NM NS 0 PS PM PB*}*. The discourse universes for the inputs are [-6 6]. Considering that the increment of PID parameters is small, the discourse universes for the outputs are [-1 1].

The membership functions μ for the inputs and the outputs are shown in Fig.19 and Fig.20, respectively.

According to the fuzzy rules in [3], the tuning of Δe_p, Δe_i, and Δe_d uses the following three rules of thumb;

If $|e|$ is larger, then Δe_p should be larger and Δ smaller, so the system responds quickly.

Meanwhile, the integral action should be limited, usually, Δe_i =0, to avoid the system appearing large overshoot.
If $|e|$ is moderate, then Δ should be smaller; the value of Δe_d is more important to obtain a small overshoot.
If $|e|$ is smaller, then Δex_p and Δe_i should be larger to improve the system's steady-state performance. When $|e(\dot{t})|$ is smaller, Δe_d should be larger. When $|e(\dot{t})|$ is larger, Δe_d should be smaller. In such a way, the system can avoid oscillation near the set point.
The control strategy in the proposed AFPIDC can be given as follows;
if e is (…) and $e(\dot{t})$ is (…), then Δe_p is (…), Δe_i is (…) and Δe_d is (…).

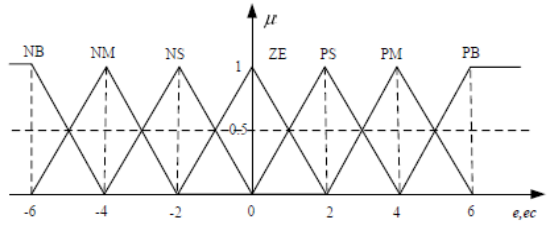

Figure 22. The membership function of e(t) , $e(\dot{t})$.

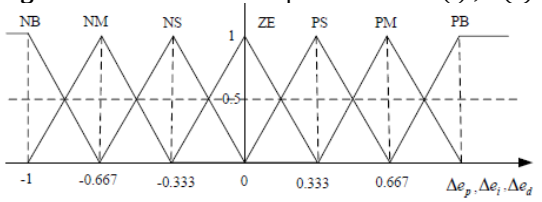

Figure 23. The membership function of Δe_p, Δe_i, and Δe_d.

The fuzzy rules to compute Δep(t), Δei(t), and Δed(t) are tabulated in Table I, Table II, and Table III, respectively.

Table 4. Self-tuning Fuzzy PID rules for Δep(t).

de(t)/dt								
e(t)		NL	NM	NS	ZR	PS	PM	PL
	NL	PL	PL	PM	PM	PS	ZR	ZR
	NM	PL	PL	PM	PS	PS	ZR	NS
	NS	PM	PM	PM	PS	ZR	NS	NS
	ZR	PM	PM	PS	ZR	NS	NM	NM
	PS	PS	PS	ZR	NS	NS	NM	NM
	PM	PS	ZR	NS	NM	NM	NM	NB
	PL	ZR	ZR	NM	NM	NM	NB	NB

Table 5. Self-tuning Fuzzy PID rules for $\Delta e_i(t)$.

de(t)/dt								
e(t)		NL	NM	NS	ZR	PS	PM	PL
	NL	NB	NB	NM	NM	NS	ZR	ZR
	NM	NB	NB	NM	NS	NS	ZR	ZR
	NS	NB	NM	PS	NS	ZR	PS	PS
	ZR	NM	NM	NS	ZR	PS	PM	PM
	PS	NM	NS	ZR	PS	PS	PM	PB
	PM	ZR	ZR	PS	PS	PM	PB	PB
	PL	ZR	ZR	PS	PM	PM	PB	P. B.

Table 6. Self-tuning Fuzzy PID rules for $\Delta e_d(t)$.

de(t)/dt								
e(t)		NL	NM	NS	ZR	PS	PM	PL
	NL	PS	NS	NB	NB	NB	NM	PS
	NM	PS	NS	NB	NM	NM	NS	ZR
	NS	ZR	NS	NM	NM	NS	NS	ZR
	ZR	ZR	NS	NS	NS	NS	NS	ZR
	PS	ZR	ZR	ZR	ZR	ZR	ZR	ZR
	PM	PM	NS	PS	PS	PS	PS	PB
	PL	PB	PM	PM	PM	PS	PS	PB

The results of this section are given below;

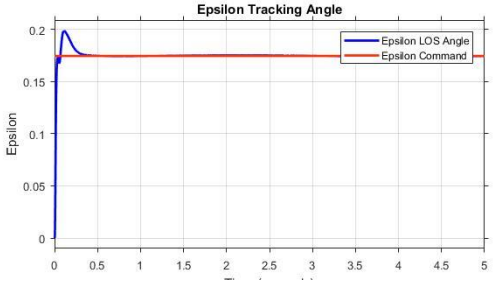

Figure 24. Elevation angle step response

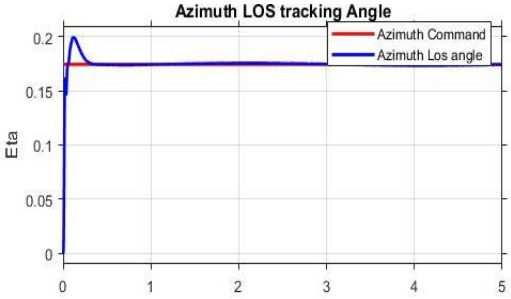

Figure 25. Azimuth angle step response

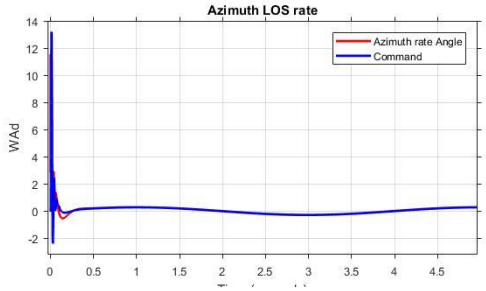

Figure 26. Azimuth rate angle response

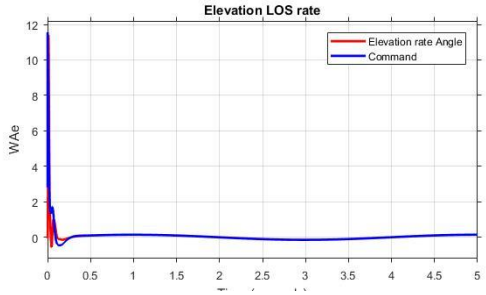

Figure 27. Elevation rate angle response.

Analysis and Comparison

Different Control method for Error Tracking

For low base angular rates such as wpi=5 rad/s, wpj=10 rad/s, and wpk=15 rad/s, the error of tracking angles on elevation and azimuth channel will be shown as follows;

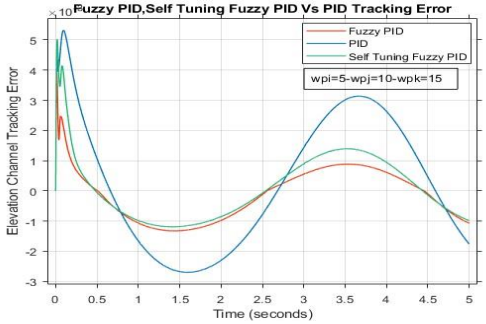

Figure 28. Elevation channel tracking error(wpi=5,wpj=10,wpk=15).

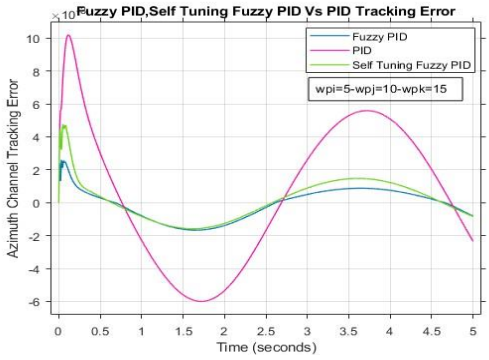

Figure 29. Azimuth channel tracking error (wpi=5,wpj=10,wpk=15).

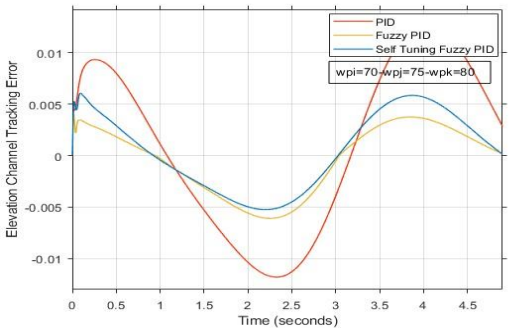

Figure 30. Elevation channel tracking error (wpi=70,wpj=75,wpk=80).

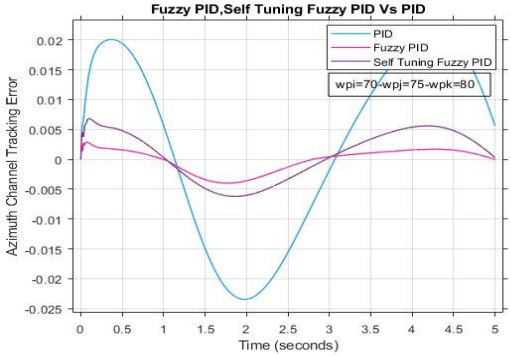

Figure 31. Azimuth channel tracking error (wpi=70,wpj=75,wpk=80).

From the figures above, it is clear that PID has the most error, and Fuzzy PID has the minor error for platform control.

Angular rate error versus different base angular rate

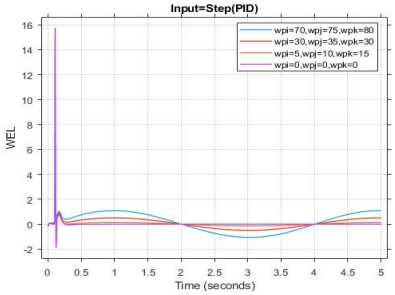

Figure 32. Elevation channel angular rate error

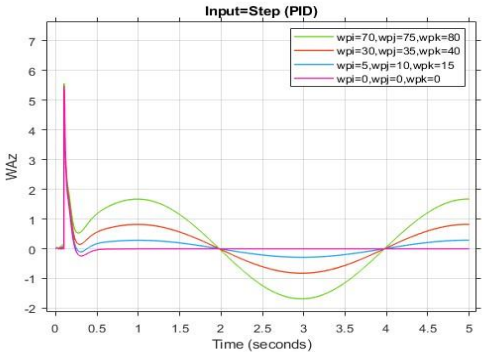

Figure 33. Azimuth channel angular rate error

Tracking error versus different base angular rate

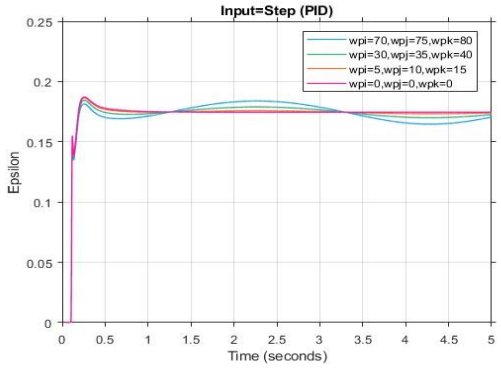

Figure 34. Elevation channel tracking error

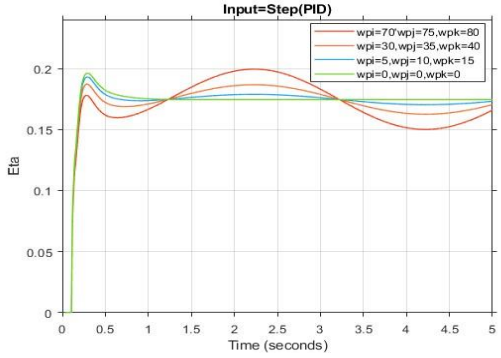

Figure 35. Azimuth channel tracking error

It is understood from 6.2 and 6.3 that the error of tracking and angular rate will be increased by the angular base rate getting more.

Tracking error versus different platform unbalancing

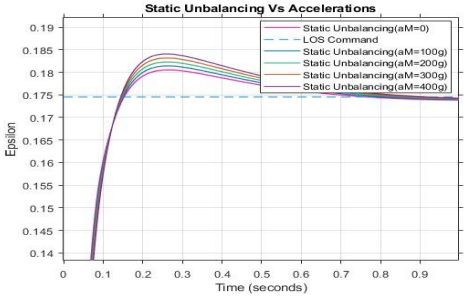

Figure 36. Elevation channel tracking error

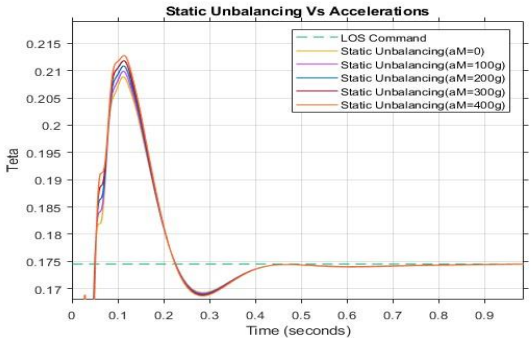

Figure 37. Azimuth channel tracking error.

Angular rate error versus different platform unbalancing

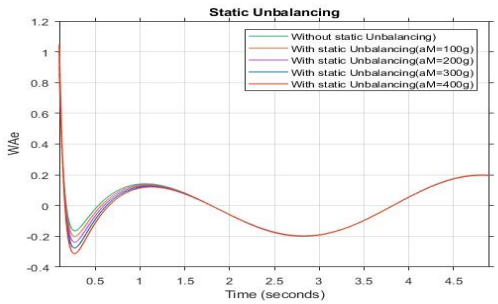

Figure 38. Elevation channel angular rate error

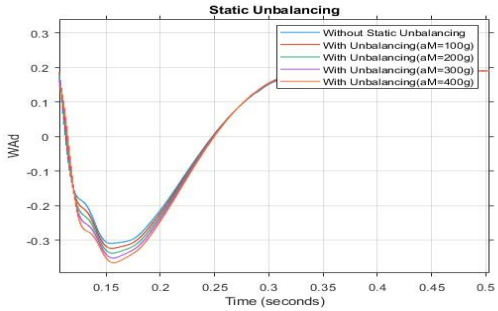

Figure 39. Azimuth channel angular rate error

According to Sections 6.4 and 6.5, it is found that the tracking errors and the angular rate both increase with increasing unbalance

Tracking error versus different Offset Distance

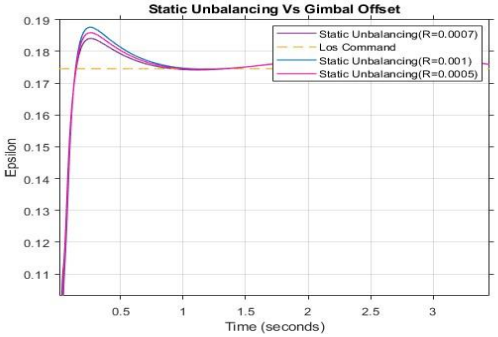

Figure 40. Elevation channel tracking error

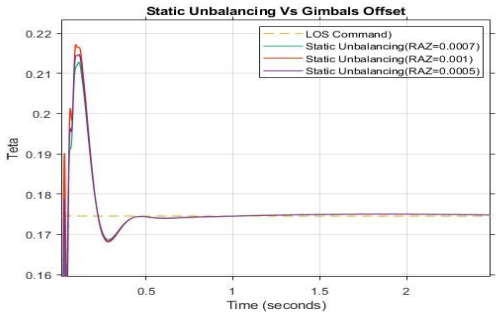

Figure 41. Azimuth channel tracking error

Angular rate error versus different Offset Distance

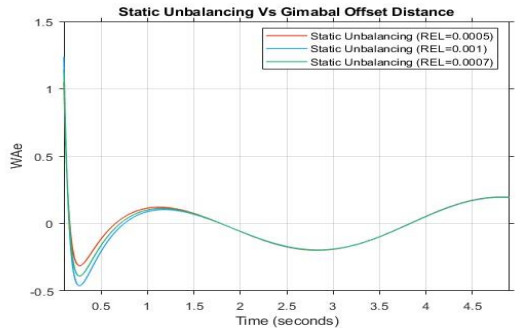

Figure 42. Elevation channel angular rate error

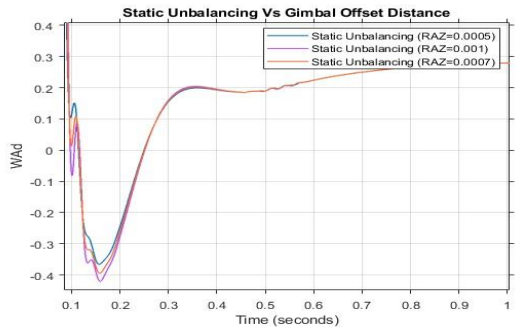

Figure 43. Azimuth channel angular rate error

Sections 6.6 and 6.7 shows if the offset increases, the error will also increase**.**

A summary of the numerical results of the above figures will be shown in 3 tables as follow;

Table 7. Different control method tracking error for wpi=5,wpj=10,wpk=15

wpi=5rad/s wpj=10rad/s wpk=15rad/s			
Control method	PID	Fuzzy PID	Self Tuning
Elevation tracking error	5.5×10^{-8}	1.5×10^{-8}	3.1×10^{-8}
Azimuth tracking error	4.2×10^{-8}	0.5×10^{-8}	2.3×10^{-8}
Elevation Angular rate error	0.3564	0.2363	0.4243
Azimuth Angular rate error	0.4220	0.2548	0.3541

Table 8. Different control method tracking error for wpi=30,wpj=35,wpk=40

wpi=30rad/s wpj=35rad/s wpk=40rad/s			
Control method	PID	Fuzzy PID	Self Tuning
Elevation tracking error	4×10^{-4}	1.8×10^{-6}	2.1×10^{-5}
Azimuth tracking error	1.8×10^{-4}	2.25×10^{-5}	1.5×10^{-4}
Elevation Angular rate error	0.4232	0.3031	0.4919
Azimuth Angular rate error	0.5213	0.4030	0.4206

Table 9. Different control method tracking error for wpi=70,wpj=75,wpk=80.

wpi=70rad/s wpj=75rad/s wpk=80rad/s			
Control method	PID	Fuzzy PID	Self Tuning
Elevation tracking error	2.5×10^{-4}	1.2×10^{-4}	3.1×10^{-4}
Azimuth tracking error	4.9×10^{-4}	1.01×10^{-4}	4.5×10^{-4}
Elevation Angular rate error	0.6432	0.4231	0.5069
Azimuth Angular rate error	0.6250	0.4459	0.5236

Calculating Bandwidth From Time Domain Response

For the elevation channel, from the step response of tracking angle, rise time and overshoot will be found as follows;

$t_r = 88ms$

$O.V = 3.64\% = 0.036$

From overshoot, ζ can be calculated as follow;

$$O.V = e^{\frac{-\pi\zeta}{\sqrt{1-\zeta^2}}} \rightarrow \zeta = 0.7$$

After that, ω_d, ω_n will be calculated by the formula below;

$$t_r = \frac{\pi - \cos^{-1}\zeta}{\omega_d} \rightarrow \omega_d = 26.7\frac{rad}{s}$$

$$\omega_n = \frac{\omega_d}{\sqrt{1-\zeta^2}} \rightarrow \omega_n = 10\, rad/s$$

$$B.W = \omega_n\sqrt{(1-2\zeta^2) + \sqrt{4\zeta^4 - 4\zeta^2 + 2}}$$

$$B.W = 10\frac{rad}{s} \rightarrow f = \frac{\omega}{2\pi} = 1.5Hz$$

So, the bandwidth of the elevation channel found as 1.5Hz.

By similar calculation, when;

$t_r = 13ms$

$O.V = 16.6\% = 0.166$

The bandwidth of the azimuth channel will be calculated as 3Hz.

This issue has been proven in the following bode diagrams.

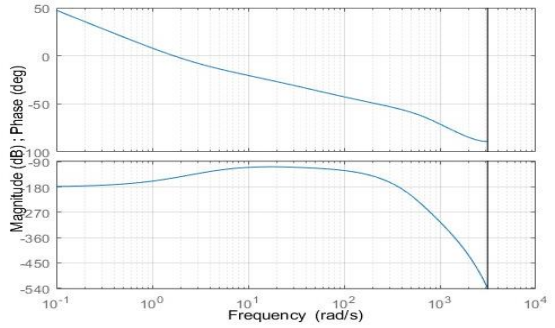

Figure 44. Bode plot of the Elevation channel

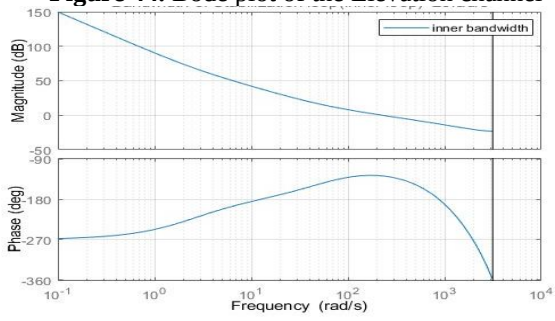

Figure 45. Bode plot of Azimuth channel

Conclusion

The results of this paper can be summarized as follows;

First, the performance of the Fuzzy PID controller is much better than the PID controller in all angular velocities caused by mechanical disturbances applied to the platform in three directions.

Second, the performance of the Fuzzy PID controller is better than the Self Tuning Fuzzy PID controller in all angular velocities caused by mechanical disturbances applied to the platform in three directions.

Third, at high angular velocities of the platform caused by mechanical disturbances, the performance of Fuzzy PID and Self Tuning Fuzzy PID controllers is much better than PID controllers.

Forth, with the increase of the aforementioned angular speeds, the performance of the fuzzy controllers is wholly preserved and stable so that the gimbals angle tracking error does not

change, but the error increases significantly in the case of the PID controller.

Fifth, if a step input is entered into the system, we will have an overshoot in torque and angular velocity. Still, no overshoot was observed if a sinusoidal input is entered, which is also slow and smooth.

Sixth, the final torque produced by the motors is such that within a few seconds, the torques caused by mechanical disturbances are zero, and the platform returns to its previous position and keeps stable.

References

[1] D.-Q. T., Y.-B. K. a. S. C. DongHun Lee, "A Robust Double Active Control System Design for Disturbance Suppression of a Two-Axis Gimbal System," *electronics*, vol. 9, no. 10, pp. 1-18, 2020.

[2] B. Ekstrand, "Equations of motion for a two-axes gimbal system," *IEEE Transactions on Aerospace and Electronic Systems*, vol. 37, no. 3, pp. 1083-1091, 2001.

[3] S. S. K. a. G. Anitha, "A Novel Self-Tuning Fuzzy Logic-Based PID Controllers for Two-Axis Gimbal Stabilization in a Missile," *International Journal of Aerospace Engineering*, vol. 2021, no. https://doi.org/10.1155/2021/8897556, pp. 1-12, 2021.

[4] R. A.K., "Precision stabilization systems," *IEEE Trans. Aerospace and Electronic Systems*, vol. 10, no. 1, pp. 34-42, 1974.

[5] Y. S. a. Z. Y., "A New measurement method for unbalanced moments in two axes gimbaled seeker," *Chinese Journal of Aeronautics*, vol. 23, no. 1, pp. 117-122, 2010.

[6] K. H., "Robust control and modeling a 2-DOF Inertial Stabilized Platform," in *International Conference on Electrical, Control and Computer engineering*, Pahang, Malaysia, 2011.

[7] X. a. M. C. Chen, "Precise control of a magnetically suspended double-gimbal control moment gyroscope using differential geometry decoupling method," *Chinese Journal of Aeronautics*, vol. 26, no. 4, pp. 1017-1028, 2013.

[8] R. V. A. T. a. M. R. A. Abdo Maher, "Research on the cross-coupling of a two axes gimbal system with dynamic unbalance," *International Journal of advanced robotic systems*, vol. 10, no. 10, pp. 357-370, 2013.

[9] S. B. S. H. K. a. Y. K. K. Kim, "Robust control for a two-axis gimbaled sensor system with multivariable feedback systems," *IET control theory & applications*, vol. 4, no. 4, pp. 539-551, 2010.
[10] a. M. T. Naderolasli, "Stabilization of the two-axis gimbal system based on an adaptive fractional-order sliding-mode controller," *IETE Journal of Research*, vol. 63, no. 1, pp. 124-133, 2017.
[11] X. H. Z. a. R. Y. Zhou, "Decoupling control for two-axis inertially stabilized platform based on an inverse system and internal model control," *Mechatronics*, vol. 24, no. 8, pp. 1203-1213, 2014.
[12] J. R. Y. a. X. L. Fang, "An adaptive decoupling control for three-axis gyro stabilized platform based on neural networks," *Mechatronics*, vol. 27, no. 1, pp. 38-46, 2015.
[13] W. S. a. J. N. Qadir, "Vision-based neuro-fuzzy controller for a two axes gimbal system with small UAV," *Journal of Intelligent & Robotic Systems*, vol. 74, no. 4, pp. 1029-1047, 2014.
[14] a. M. T. Naderolasli, "Two-axis Gimbal System Stabilization Using Adaptive Feedback Linearization," *Recent Advances in Electrical & Electronic Engineering*, vol. 12, no. 1, pp. 1-11, 2019.
[15] D. H. M. D. Bo Li, "Nonlinear Induced Disturbance Rejection in Inertial Stabilization Systems," *IEEE Transactions on control systems technology*, vol. 6, no. 3, 1998.
[16] Z. Q. R. J. H. Ambrose, "Nonlinear Robust Control For A Passive Line-of-Sight stabilization system," in *Proceedings of the 2001 IEEE International Conference on Control Applications*, Mexico, 2001.
[17] E. K. M. L. T.H. Lee, "stable adaptive control of multivariable servomechanism with application to a passive line-of-sight stabilization system," *IEEE Transactions on Industrial Electronics*, vol. 43, no. 1, pp. 98-105, 1996.
[18] D. H. Bo Li, "Self-Tuning Controller for Nonlinear Inertial Stabilization System," *IEEE Transactions on control systems technology*, vol. 6, no. 3, 1998.
[19] H.-G. K. B.-Y. Y. a. H.-P. L. K.-J. Seong, "The stabilization loop design for a two-axis gimbal system using LQG/LTR controller," *in Proc.SICE-ICASE Int. Joint Conf., 2006*, 2006.
[20] S. C. D. K. a. H. S. K. Deng, "Discrete-time direct model reference adaptive control application in a high-precision inertially stabilized platform," *IEEE Trans. Ind. Electron.*, vol. 66, no. 1, pp. 358-367, 2018.
[21] M. R. a. Z. Hurák, "Structured MIMO H1 design for dual-stage inertial stabilization: A case study for HIFOO and Hinfstruct solvers," *Mechatronics*, vol. 23, no. 8, pp. 1084-1093, 2013.
[22] H. L. H. Z. a. X. M. M. Zhang, "A hybrid control strategy for the optoelectronic stabilized platform of a seeker," *Optik*, vol. 181, no. 1, pp. 1000-1012, 2019.
[23] A., A., M. A. Maher Mahmoud Abdo, "Stabilization loop of a two axes gimbal system using self-tuning PID type fuzzy controller," *ISA Transactions*, vol. 53, no. 2, pp. 591-602, 2014.
[24] P. Kennedy and R. Kennedy, "Direct versus indirect line of sight (LOS) stabilization," *IEEE Trans on control system technology*, vol. 11, pp. 3-15, 2003.
[25] H. TangKZ, "Combined PID and adaptive nonlinear control for mechanical servo systems," *Mechatronics*, vol. 14, no. 6, pp. 701-714, 2004.
[26] S. Malhotra, "Design of Embedded Hybrid Fuzzy-GA Control," *International Journal of Computer Applications*, vol. 6, no. 5, pp. 37-46, 2010.
[27] M. S.A., "Design and Simulation of Servomechanism for Rate Gyro Stabilized Seeker," MUT, Tehran, 2010.
[28] J. Hilkert, "Adaptive control system techniques applied to inertial stabilization systems," in *In: Proceedings of SPIE Conference*, 1990.
[29] M. Abdo, "Modeling and Control of A two Axes Gimbal Seeker," Malek Ashtar University, Tehran, 2014.
[30] M. Khuntia SR, "A comparative study of P–I, I–P, fuzzy and neuro-fuzzy controllers for speed control of D.C. motor drive," *World Academy of Science*, vol. 44, pp. 525-529, 2010.
[31] H. N. M. S. Wahid N, "Application of intelligent controller in the feedback control loop for aircraft pitch control," *Aust J Basic Appl Sci*, no. 5, pp. 1065-74, 2011.
[32] Y. E. M. I. Karasakal O, "Implementation of a new self-tuning fuzzy PID controller on PLC," *Turk J Elec Engin*, vol. 13, pp. 277-86, 2005.
[33] M. Qiao W, "PID type fuzzy controller and parameters adaptive method," *FuzzySetsSyst*, vol. 78, pp. 23-35, 1996.
[34] H. Fujita, "Torque control for D.C. servo motor using adaptive load," in *Proceedings of the ninth WSEAS international conference*, 2010.